Mechanism of the Reaction Catalyzed by Isoaspartyl Dipeptidase from *Escherichia coli*[†,‡]

Ricardo Martí-Arbona,[§] Vicente Fresquet,[§] James B. Thoden,[||] Melissa L. Davis,[||] Hazel M. Holden,[||] and Frank M. Raushel*[,§]

Department of Biochemistry, University of Wisconsin, Madison, Wisconsin 53706, and Department of Chemistry, P.O. Box 30012, Texas A&M University, College Station, Texas 77842-3012

Received January 3, 2005; Revised Manuscript Received March 16, 2005

ABSTRACT: Isoaspartyl dipeptidase (IAD) is a member of the amidohydrolase superfamily and catalyzes the hydrolytic cleavage of β-aspartyl dipeptides. Structural studies of the wild-type enzyme have demonstrated that the active site consists of a binuclear metal center positioned at the C-terminal end of a $(\beta/\alpha)_8$-barrel domain. Steady-state kinetic parameters for the hydrolysis of β-aspartyl dipeptides were obtained at pH 8.1. The pH−rate profiles for the hydrolysis of β-Asp-Leu were obtained for the Zn/Zn-, Co/Co-, Ni/Ni-, and Cd/Cd-substituted forms of IAD. Bell-shaped profiles were observed for k_{cat} and k_{cat}/K_m as a function of pH for all four metal-substituted forms. The pK_a of the group that must be unprotonated for catalytic activity varied according to the specific metal ion bound in the active site, whereas the pK_a of the group that must be protonated for catalytic activity was relatively independent of the specific metal ion present. The identity of the group that must be unprotonated for catalytic activity was consistent with the hydroxide that bridges the two divalent cations of the binuclear metal center. The identity of the group that must be protonated for activity was consistent with the free α-amino group of the dipeptide substrate. Kinetic constants were obtained for the mutant enzymes at conserved residues Glu77, Tyr137, Arg169, Arg233, Asp285, and Ser289. The catalytic properties of the wild-type and mutant enzymes, coupled with the X-ray crystal structure of the D285N mutant complexed with β-Asp-His, are consistent with a chemical reaction mechanism for the hydrolysis of dipeptides that is initiated by the polarization of the amide bond via complexation to the β-metal ion of the binuclear metal center. Nucleophilic attack by the bridging hydroxide is facilitated by abstraction of its proton by the side chain carboxylate of Asp285. Collapse of the tetrahedral intermediate and cleavage of the carbon−nitrogen bond occur with donation of a proton from the protonated form of Asp285.

Isoaspartyl dipeptidase (IAD)[1] from *Escherichia coli* catalyzes the hydrolysis of dipeptides containing a peptide bond to the β-carboxylate group of aspartic acid (*1*). Isoaspartyl peptide bonds are formed via an intramolecular rearrangement of the polypeptide backbone of proteins at amide bonds to asparagine (*2*). The apparent physiological role of IAD in *E. coli* is to prevent the accumulation of β-aspartyl dipeptides after proteolysis of these proteins. The enzyme displays little activity, however, toward the hydrolysis of tripeptides or γ-glutamyl dipeptides (*2*). The general reaction catalyzed by IAD is presented in Scheme 1. The sequence of the enzyme is significantly similar to the sequences of members of the amidohydrolase superfamily and most closely resembles those of dihydroorotase and

Scheme 1

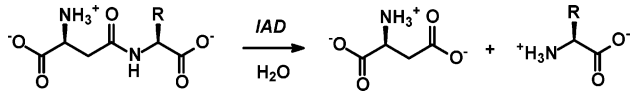

D-hydantoinase (*2*−*6*). Other members within the amidohydrolase superfamily have been found to catalyze the hydrolysis of amides and ester bonds at phosphorus and carbon centers (*7*). The hallmark for proteins in this superfamily is a mononuclear or binuclear metal center embedded at the C-terminal end of a $(\beta/\alpha)_8$-barrel core.

The three-dimensional structure of IAD from *E. coli* was recently determined, both in the presence and in the absence of the hydrolysis product, aspartate (*3*). From this investigation, the quaternary structure of the protein was shown to be an octamer with each subunit folding into two domains as displayed in Figure 1. The first domain, composed of eight strands of mixed β-sheet, is followed by a $(\beta/\alpha)_8$-barrel motif, which houses the binuclear metal center. The α-metal of the binuclear center is coordinated by His68, His70, Lys162, Asp285, and the bridging solvent, whereas the β-metal is surrounded in a tetrahedral arrangement by Lys162, His201, His230, and the bridging solvent. The ϵ-amino group of Lys162 has reacted to form a carbamate functional group that serves as a bridging ligand between the two metal ions.

[†] This work was supported in part by the NIH (Grant GM 33894). R.M.-A. was supported as a trainee of the Chemistry-Biology Interface Training Program (T32GM 008523). M.L.D. is a recipient of a predoctoral fellowship from the National Science Foundation.

[‡] X-ray coordinates have been deposited in the Research Collaboratory for Structural Bioinformatics Protein Data Bank as entry 1YBQ.

* To whom correspondence should be addressed. Phone: (979) 845-3373. Fax: (979) 845-9452. E-mail: raushel@tamu.edu.

[§] Texas A&M University.

[||] University of Wisconsin.

[1] Abbreviations: HEPES, *N*-(2-hydroxyethyl)piperazine-*N*′-2-ethanesulfonic acid; IAD, isoaspartyl dipeptidase; WT, wild type.

10.1021/bi050008r CCC: $30.25
Published on Web 04/19/2005

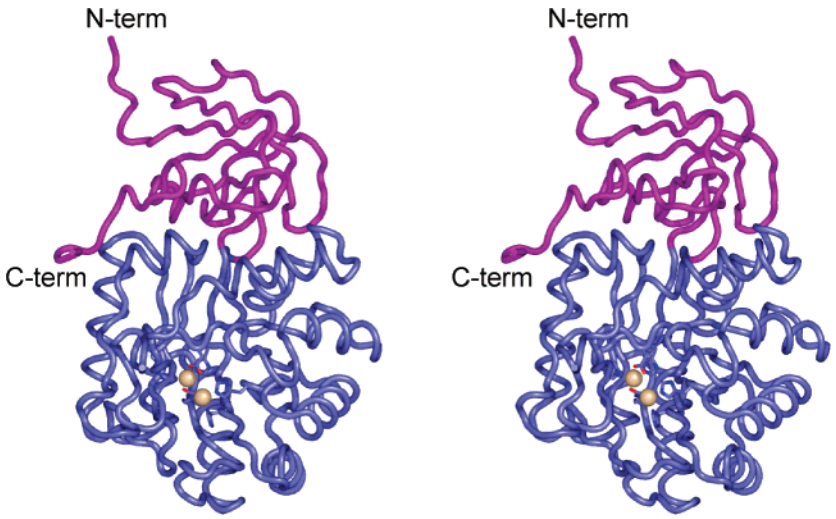

FIGURE 1: Structure of IAD from *E. coli*. The quaternary structure of IAD is octameric. Shown is a trace of one subunit with the N- and C-terminal domains colored magenta and slate, respectively.

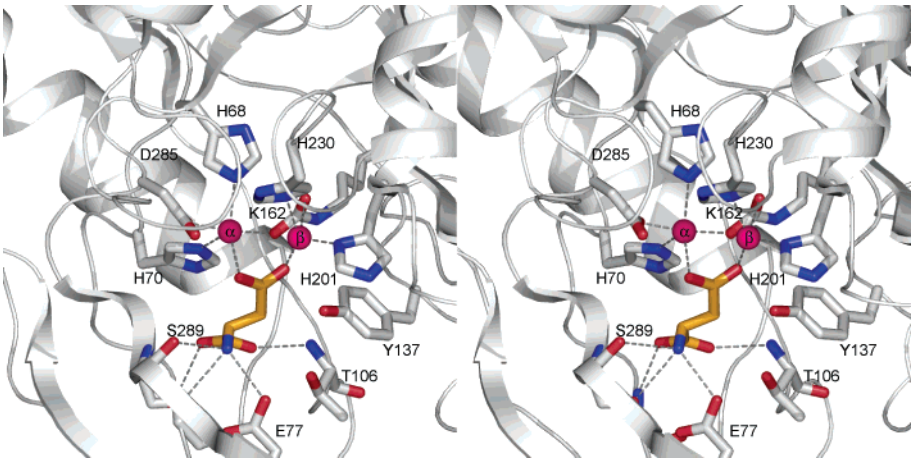

FIGURE 2: Close-up view of the active site of IAD with bound aspartate, highlighted with gold bonds.

The initial three-dimensional models of IAD provided significant insight into those amino acid residues likely to be important for substrate binding and/or catalytic activity. For example, Tyr137 was shown to sit 3.4 Å from the β-metal ion, while Glu77 was in the proper position to form an ion pair with the α-amino group of the dipeptide substrate (*3*). In the structure of IAD complexed with aspartate, the side chain carboxylate group of the amino acid product was shown to displace the bridging solvent molecule (*3*). Additionally, the IAD−aspartate complex structure demonstrated that ligand binding to the enzyme induces a movement of the Phe292−His301 loop toward the active site, resulting in the formation of a hydrogen bond between O^{γ} of Ser289 and the α-amino group of the bound aspartate ligand. The coordination geometry of the binuclear metal center and the binding interactions of the aspartate product are presented in Figure 2.

While these initial structures were informative, there are still a number of unresolved questions regarding the mechanism of the reaction catalyzed by IAD. It is unclear how the hydrolytic water molecule is activated or how the β-aspartyl peptide bond is polarized for nucleophilic attack. In addition, the structural determinants to the substrate specificity have not been elucidated. It is also uncertain how the catalytic mechanism of this protein might differ from those of other homologous enzymes within the amidohydrolase superfamily. In the investigation reported here, the enzyme has been reconstituted with a variety of divalent cations to probe the activation of the hydrolytic water molecule. A series of dipeptides, substrate analogues, and other inhibitors have also been synthesized as reporters for ligand binding requirements, and a number of active site mutant proteins have been constructed to ascertain the role of specific amino acids with regard to substrate binding and catalysis. Finally, the structure of the D285N site-directed mutant protein complexed with β-Asp-His has been determined and refined to 2.0 Å resolution.

EXPERIMENTAL PROCEDURES

Materials. All chemicals, dipeptides, substrate analogues, and coupling enzymes were obtained from Sigma or Aldrich, unless otherwise stated. The dipeptides β-Asp-Leu (**I**), α-Asp-Leu (**II**), β-Asp-Lys, β-Glu-Leu, and β-Asp-Ala were purchased from Bachem. The structures for some of the substrates and inhibitors are presented in Scheme 2.

Cloning and Site-Directed Mutagenesis. The *iad*A gene was cloned from the XL1Blue strain of *E. coli* into a pET30 plasmid as previously described (*3*). Site-directed mutagenesis of IAD at residues Glu77, Tyr137, Arg169, Arg233, Asp285, and Ser289 was accomplished using the Quick Change site-directed mutagenesis kit from Stratagene. For

Scheme 2

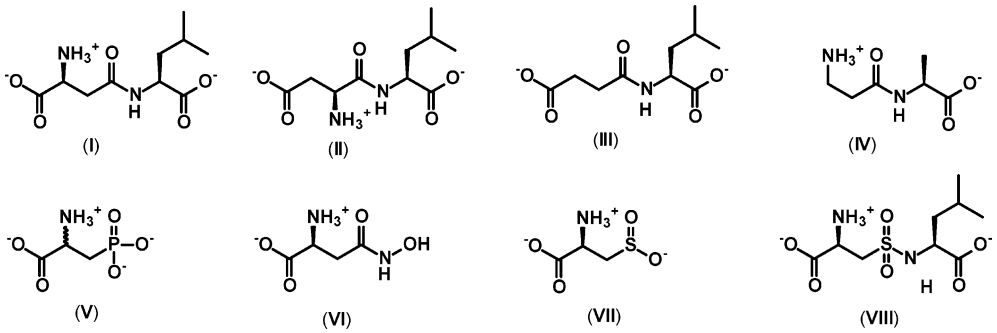

expression of the IAD mutants, JDG 11000 cells (Δ*iad*A) were lysogenized using the *λ*DE3 lysogenization kit from Novagen. *E. coli* strain JDG 11000 (Δ*iad*A) that lacks a functional *iad*A gene was kindly provided by S. Clarke at the University of California (Los Angeles, CA) (*2*).

Protein Purification. BL21(DE3)star cells (Novagen) were transformed by the pET30 plasmid encoding IAD. Cultures were grown in Luria−Bertani medium at 37 °C, induced by the addition of 1.0 mM IPTG after an A_{600} of 0.6 had been reached, and shaken overnight. The cells were centrifuged and resuspended in 20 mM HEPES buffer at pH 8.1 (buffer A) containing 5 *μ*g/mL RNAse and 0.1 mg/mL phenylmethanesulfonyl fluoride. The cells were disrupted by sonication, and the soluble protein was isolated from the lysed cells by centrifugation and subsequently fractioned between 20 and 50% saturation of ammonium sulfate in buffer A. The precipitated protein was resuspended in a minimum quantity of buffer A, loaded onto a Superdex 200 gel filtration column (Amersham Pharmacia), and eluted with buffer A. The fractions containing IAD were pooled, loaded onto a Resource Q anion exchange column (Amersham Pharmacia), and eluted with a gradient of NaCl in buffer A. The protein from the active fractions was pooled, precipitated with ammonium sulfate, and then rechromatographed on the Superdex 200 gel filtration column. The chromatographic profiles on the gel filtration columns were the same for the wild-type enzyme and all of the mutants, indicating that the quaternary structure was not perturbed by any of the amino acid changes. The purified enzyme was stored at −20 °C.

*Synthesis of Succinyl-L-Leucine (**III**).* L-Leucine benzyl ester (1.84 g, 8.3 mmol) was added to a solution of succinic anhydride (1.0 g, 10 mmol) and 4-(dimethylamino)pyridine (1.02 g, 8.3 mmol) in CH_2Cl_2 (300 mL). After being stirred at room temperature for 5 h, the reaction mixture was extracted three times with 300 mL of a 5% solution of sodium bicarbonate. The aqueous phase was acidified with 6 N HCl and extracted with ethyl acetate. The ethyl acetate layer was washed with brine, dried over sodium sulfate, and concentrated to dryness under vacuum. The succinyl-L-leucine benzyl ester was obtained as a colorless syrup (1.50 g) with a 56% yield: ESI-MS *m*/*z* 320.2 [M − H], 356.0 [M + Cl]; ^{1}H NMR ($CDCl_3$) *δ* 7.36 (s, 5H), 5.85 (d, J = 12 Hz, 1H), 5.12 (d, J = 18 Hz, 2H), 4.68 (q, J = 12 Hz, 1H), 3.92 (m, 4H), 3.04 (m, 1H), 2.97 (m, 2H), 2.30 (d, J = 6.5, 3H), 2.26 (d, J = 6.5, 3H); ^{13}C NMR ($CDCl_3$) *δ* 176.74, 172.94, 171.66, 135.16, 128.59, 128.45, 128.22, 67.20, 50.95, 41.48, 30.48, 29.64, 29.37, 24.77, 22.71, 21.87.

The unprotected succinylleucine was prepared by hydrogenation of the succinyl-L-leucine benzyl ester (0.80 g, 3.5 mmol) using 50 mg of Pd/C in 30 mL of methanol and H_2 gas with constant stirring. After 5 h, the Pd/C was removed by filtration and the sample taken to dryness under vacuum. The succinylleucine was obtained as a colorless syrup (0.68 g) with an 85% yield: ESI-MS *m*/*z* 230.1 [M − H]; ^{1}H NMR (methanol) *δ* 4.68 (q, J = 12 Hz, 1H), 3.92 (m, 4H), 3.09 (m, 1H), 2.99 (m, 2H), 2.33 (d, J = 6.5, 3H), 2.29 (d, J = 6.5, 3H); ^{13}C NMR (acetone) *δ* 52.38, 49.86, 49.57, 49.22, 49.00, 48.72, 49.44, 48.15, 41.70, 31.35, 30.23, 25.99, 23.40, 21.78.

*Synthesis of 3-Sulfo-L-Alanine-S-L-Leucine (**VIII**).* L-Leucine benzyl ester (0.55 g, 1.4 mmol) and 0.42 *μ*L (1.4 mmol) of Et_3N were dissolved in 10 mL of chloroform at 4 °C under constant stirring. *N*-Carbobenzoxy-3-(sulfonylchloro)-L-alanine benzyl ester (0.39 g, 0.95 mmol) dissolved in 10 mL of chloroform was added slowly (*8*). The mixture was allowed to reach room temperature and stirred for 3 h. The reaction mixture was taken to dryness under vacuum. The colorless syrup was resuspended in a minimal amount of mixed hexanes, loaded onto a silica column, and eluted with a 5:1 hexanes/ethyl acetate mixture. The product was taken to dryness and crystallized from a 5:1 hexanes/ethyl acetate mixture to yield 0.13 g of *N*-carbobenzoxy-3-sulfo-L-alanine-*S*-L-leucine dibenzyl ester (24% yield): ESI-MS *m*/*z* 597.2 [M + H]; ^{1}H NMR ($CDCl_3$) *δ* 7.37 (br s, 10H), 6.08 (d, J = 6.6, 1H), 5.17 (d, J = 18 Hz, 2H), 5.13 (d, J = 18 Hz, 2H), 5.02 (d, J = 6.6 Hz, 1H) 4.82 (q, J = 12 Hz, 1H), 4.16 (m, 1H), 3.47 (m, 1H), 1.87 (m, 2H), 1.50 (d, J = 6.5 Hz, 3H), 0.90 (d, J = 6.5 Hz, 3H), 0.877 (d, J = 6.5 Hz, 3H); ^{13}C NMR ($CDCl_3$) *δ* 172.95, 171.67, 170.12, 168.68, 128.95, 128.78, 128.42, 68.92, 67.65, 65.29, 50.99, 41.48, 30.49, 29.64, 29.38, 24.78, 22.71, 21.87.

The unprotected product was prepared by mixing *N*-carbobenzoxy-3-sulfo-L-alanine-*S*-L-leucine dibenzyl ester (0.134 g, 0.5 mmol) with 50 mg of Pd/C in 15 mL of methanol, and H_2 gas was bubbled with constant stirring. After 4 h, the Pd/C was filtered and the solvent was removed under vacuum. The 3-sulfo-L-alanine-*S*-L-leucine was obtained as a colorless syrup (46 mg) in 72% yield: ESI-MS *m*/*z* 283.09 [M + H]; ^{1}H NMR (D_2O) *δ* 4.03 (d, J = 9.3 Hz, 2H), 3.62 (m, 1H), 3.69 (m, 1H), 3.46 (m, 2H), 1.57 (m, 2H), 1.46 (d, J = 6.5 Hz, 3H), 0.761 (d, J = 6.5 Hz, 3H), 0.742 (d, J = 6.5 Hz, 3H); ^{13}C NMR ($CDCl_3$) *δ* 170.13, 168.67, 68.92, 65.28, 50.98, 41.48, 30.49, 29.63, 29.37, 24.76, 22.70, 21.87.

Substrate Activity. Compounds *β*-Asp-Leu (**I**), α-Asp-Leu (**II**), succinyl-Leu (**III**), *β*-Ala-Ala (**IV**), *β*-Asp-Ala, *β*-Asp-Gly, *β*-Asp-His, *β*-Asp-Lys, *β*-Asp-Phe, and *γ*-Glu-Leu were tested as substrates for IAD. The specific activity of IAD toward the hydrolysis of isoaspartyl dipeptides was followed

by coupling the formation of aspartate to the oxidation of NADH (*9*). The change in the NADH concentration was measured spectrophotometrically at 340 nm using a SPECTRAmax-340 microplate reader (Molecular Devices Inc.). The standard assay contained 100 mM HEPES (pH 8.1), 100 mM KCl, 3.7 mM α-ketoglutarate, 0.4 mM NADH, 0.64 unit of malate dehydrogenase, 6 units of aspartate aminotransferase, the isoaspartyl dipeptide, and IAD in a final volume of 250 μL at 30 °C.

The ability of IAD to hydrolyze γ-Glu-Leu was determined in an assay that coupled the formation of glutamate to the reduction of 3-acetylpyridine adenine dinucleotide (*10*). The 200 μL assay contained 100 mM HEPES at pH 8.1, 100 mM KCl, 11.0 μg of IAD, and up to 44 mM γ-Glu-Leu. The reaction mixture was incubated at 30 °C for 30 min; the reaction was stopped by the addition of 75 μL of 10% trichloroacetic acid, and the mixture was incubated at 4 °C for 20 min. The mixture was neutralized with 14 μL of 3.0 M Tris-HCl at pH 8.1, and then 800 μL of a solution containing 100 mM HEPES at pH 6.8, 1.0 mM 3-acetylpyridine adenine dinucleotide, and 10 units of glutamate dehydrogenase were added and incubated at 30 °C for 2 h. The reaction mixture was centrifuged and the absorbance measured at 363 nm.

The ability of IAD to hydrolyze succinyl-Leu (**III**) was assayed by amino acid analysis performed by the Protein Chemistry Laboratory of Texas A&M University. Reaction mixtures contained 100 mM HEPES at pH 8.1, 100 mM KCl, 41 mM succinyl-Leu, and 3.0 μg of IAD. The reaction mixture was incubated for 1 h, and the reaction was stopped by filtering the protein with an Ultrafree centrifugal filter device (Millipore). The filtrate was analyzed for the amount of free leucine. The ability of IAD to hydrolyze β-Ala-Ala (**IV**) was assayed using alanine dehydrogenase. The reaction was monitored at 500 nm, and the mixture contained 100 mM Hepes at pH 8.1, 1.5 mM *p*-iodonitrotetrazolium violet, 1.5 mM NAD^+, 2.0 units of diaphorase, 7.0 units of L-alanine dehydrogenase, the appropriate substrate or inhibitor, and 64 ng of IAD in a final volume of 250 μL at 30 °C (*11*).

Inhibition by Substrate Analogues. Substrate and product analogues were tested as inhibitors of the IAD reaction. Succinyl-Leu (**III**), 3-sulfo-L-Ala-*S*-L-Leu (**VIII**), and β-Ala-Ala (**IV**) were tested as inhibitors using the assay that monitors the formation of aspartate with β-Asp-Leu as the substrate. 3-Phosphono-D,L-Ala (**V**), β-Asp-hydroxamate (**VI**), L-cysteinesulfinic acid (**VII**), and β-methyl aspartate were tested as inhibitors using the assay that monitors the formation of alanine with β-Asp-Ala as the substrate.

Metal Analysis. The role of the metal ions in the IAD active site was investigated by the preparation and reconstitution of apo-IAD. IAD (1.0 mg/mL) was treated with 3.0 mM dipicolinate at 4 °C and pH 5.6 for 72 h. The chelator was removed by passing the protein through a PD10 column (Amersham Biosciences) and eluted with metal-free buffer A, prepared by being passed through a column of Chelex 100 resin. The apo-IAD was reconstituted with 45 equiv of the desired metal (Zn, Co, Ni, Cd, or Mn), 50 mM $NaHCO_3$, and 100 mM HEPES at pH 7.5. The metal content of apo-IAD and the reconstituted enzymes were quantified using a Perkin-Elmer AAnalyst 700 atomic absorption spectrometer.

pH−Rate Profiles. The pH dependence of the kinetic parameters was determined for the Zn/Zn, Co/Co, Cd/Cd, and Ni/Ni forms of wild-type IAD using β-Asp-Leu as the substrate. The pH range was varied between 5.0 and 10.0 with 0.2 pH unit increments at buffer concentrations of 100 mM.

Table 1: X-ray Data Collection Statistics

resolution limits (Å)	30−2.0 (2.09−2.0)[b]
no. of independent reflections	61655 (6311)[b]
completeness (%)	91.2 (75.6)[b]
redundancy	3.8 (2.4)[b]
average I/average $\sigma(I)$	11.0 (2.1)[b]
R_{sym}[a] (%)	5.4 (20.2)[b]

[a] $R_{sym} = (\sum|I - \bar{I}|\sum I) \times 100$. [b] Value for the highest-resolution bin.

Data Analysis. The kinetic parameters, k_{cat} and k_{cat}/K_m, were determined by fitting the initial velocity data to eq 1 (*12*)

$$v/E_t = k_{cat}S/(K_m + S) \quad (1)$$

where v is the initial velocity, E_t is the enzyme concentration, k_{cat} is the turnover number, S is the substrate concentration, and K_m is the Michaelis constant. The pK values were calculated by fitting the k_{cat} or k_{cat}/K_m values to eq 2 (*12*)

$$\log y = \log\{c/[1 + (H/K_a) + (K_b/H)]\} \quad (2)$$

where c is the pH-independent value of y, K_a and K_b are the dissociation constants of the groups that ionize, and H is the hydrogen ion concentration. Competitive inhibition patterns were fitted to eq 3 (*12*)

$$v/E_t = k_{cat}S/\{K_m[1 + (I/K_i)] + S\} \quad (3)$$

where I is the inhibitor concentration and K_i is the slope inhibition constant.

Structural Analysis. Large single crystals of the D285N mutant protein were grown by the hanging drop method of vapor diffusion against precipitant solutions containing 6−8% poly(ethylene glycol) 8000, 100 mM homopipes (pH 5.0), and 50−100 mM $MgCl_2$. They contained two subunits in the asymmetric unit and belonged to space group $P42_12$ with the following unit cell dimensions: $a = b = 119.5$ Å and $c = 138.1$ Å. The crystals were harvested from the hanging drop experiments and equilibrated in a synthetic mother liquor containing 50 mM β-Asp-His. An X-ray data set was collected to 2.0 Å resolution at 4 °C with a Bruker HISTAR area detector system equipped with Supper "long" mirrors. The X-ray source was Cu Kα radiation from a Rigaku RU200 X-ray generator operated at 50 kV and 90 mA. The X-ray data were processed with XDS (*13, 14*) and internally scaled with XSCALIBRE (Rayment and Wesenberg, unpublished program). Relevant X-ray data collection statistics are presented in Table 1.

The structure was determined by difference Fourier techniques. Iterative cycles of least-squares refinement with TNT (*15*) and manual model building reduced the *R*-factor to 18.5% for all measured X-ray data from 30.0 to 2.0 Å resolution. Relevant least-squares refinement statistics are given in Table 2.

RESULTS

Substrate Specificity. A variety of compounds were tested as substrates for the bacterial IAD. The kinetic constants for

Table 2: Least-Squares Refinement Statistics

resolution limits (Å)	30.0−2.0
R-factor[a] (overall) (%) (no. of reflections)	18.5 (61655)
R-factor (working) (%) (no. of reflections)	18.1 (55612)
R-factor (free) (%) (no. of reflections)	24.3 (6043)
no. of protein atoms	5471
no. of heteroatoms[b]	283
average *B* values (Å^2)	
protein atoms	36.2
β-Asp-His	58.8
solvents	42.6
weighted rms deviations from ideality	
bond lengths (Å)	0.012
bond angles (deg)	2.3
trigonal planes (Å)	0.007
general planes (Å)	0.012
torsional angles[c] (deg)	17.1

[a] *R*-factor $= (\sum|F_o - F_c|/\sum|F_o|) \times 100$, where F_o is the observed structure factor amplitude and F_c is the calculated structure factor amplitude. [b] These include 241 water molecules, four zinc ions, and two β-Asp-His ligands. [c] The torsional angles were not restrained during the refinement.

Table 3: Kinetic Parameters for Zn/Zn-Bound IAD with Dipeptide Substrates[a]

substrate	K_m (mM)	k_{cat} (s^{-1})	k_{cat}/K_m (M^{-1} s^{-1})
β-Asp-Leu	1.02 ± 0.09	104 ± 3	(1.0 ± 0.1) × 10^5
β-Asp-Phe	0.23 ± 0.02	16.9 ± 0.4	(7.3 ± 0.7) × 10^4
β-Asp-Lys	0.91 ± 0.07	58 ± 1	(6.3 ± 0.5) × 10^4
β-Asp-Ala	3.7 ± 0.2	213 ± 5	(5.8 ± 0.3) × 10^4
β-Asp-His	3.7 ± 0.2	20.8 ± 0.7	(5.6 ± 0.7) × 10^3
β-Asp-Gly	18 ± 1	0.93 ± 0.05	(5.1 ± 0.6) × 10^1
α-Asp-Leu	5.0 ± 0.2	15.7 ± 0.2	(3.1 ± 0.1) × 10^3
β-Glu-Leu	−	−	<2.0 × 10^{-1}
succinyl-Leu	−	−	<2.0 × 10^{-1}
β-Ala-Ala	−	−	<2.0 × 10^{-1}

[a] These data were obtained at pH 8.1 at 30 °C and fit to eq 1.

the zinc-substituted form of the enzyme at pH 8.1 are presented in Table 3. In accordance with previous investigations (*1*−*3*, *16*), β-Asp-Leu (**I**) was the best substrate with a K_m of 1.0 mM and a k_{cat}/K_m of 1.0 × 10^5 M^{-1} s^{-1}. Despite the strong preference for β-aspartyl dipeptides, IAD was also able to hydrolyze α-Asp-Leu (**II**) with a K_m of 5.0 mM and a k_{cat}/K_m of 3.1 × 10^3 M^{-1} s^{-1}. The dipeptide β-Asp-Gly was found to be a relatively poor substrate with a K_m of 18 mM and a k_{cat} of 0.9 s^{-1}. Although β-Asp-Ala has the highest specific activity, the K_m value is elevated relative to those of some of the other substrates. No activity was detected with succinyl-L-Leu (**III**) or β-Ala-L-Ala (**IV**), and no turnover was found with β-Glu-L-Leu.

Inhibitors. An assortment of compounds were tested as suitable inhibitors of IAD. No inhibition could be detected with β-Ala-Ala (**IV**) up to a concentration of 29 mM. A derivative of the best substrate that lacks the free α-amino group, succinyl-L-Leu (**III**), is a weak competitive inhibitor versus β-Asp-Leu with a K_i of 134 ± 30 mM. The analogue of β-Asp-Leu that resembles the putative transition state for substrate hydrolysis, 3-sulfo-L-Ala-*S*-L-Leu (**VIII**), did not inhibit the reaction at concentrations of up to 26 mM. The three aspartate analogues, 3-phosphono-D,L-Ala (**V**), β-Asp-hydroxamate (**VI**), and L-cysteinesulfinic acid (**VII**), were all found to be competitive inhibitors versus β-Asp-Ala with K_i values of 1.5 ± 0.2, 4.7 ± 0.6, and 77 ± 9 mM, respectively.

Table 4: Kinetic Parameters for Metal-Reconstituted IAD and Mutants[a]

IAD	K_m (mM)	k_{cat} (s^{-1})	k_{cat}/K_m (M^{-1} s^{-1})
WT (Zn/Zn)	1.02 ± 0.09	104 ± 3	(1.02 ± 0.09) × 10^5
WT (Co/Co)	0.62 ± 0.03	34.0 ± 0.4	(5.5 ± 0.3) × 10^4
WT (Cd/Cd)	0.36 ± 0.05	11.9 ± 0.4	(3.3 ± 0.4) × 10^4
WT (Ni/Ni)	0.09 ± 0.01	9.2 ± 0.2	(1.0 ± 0.1) × 10^5
E77D	6.9 ± 0.9	(5.1 ± 0.3) × 10^{-3}	(7.4 ± 0.1) × 10^{-1}
E77Q	0.8 ± 0.1	(5.6 ± 0.1) × 10^{-3}	7 ± 1
Y137A	1.7 ± 0.3	(1.9 ± 0.2) × 10^{-1}	(1.1 ± 0.2) × 10^2
Y137F	1.4 ± 0.3	(1.8 ± 0.2) × 10^{-1}	(1.2 ± 0.1) × 10^2
R169K	34 ± 9	9 ± 1	(2.7 ± 0.8) × 10^2
R169M	−	−	(6.1 ± 0.1) × 10^{-2}
R233K	20 ± 2	13 ± 2	(5.3 ± 0.1) × 10^2
R233M	−	−	(6.0 ± 0.3) × 10^3
D285A	0.5 ± 0.1	(6.2 ± 0.7) × 10^{-4}	1.2 ± 0.3
D285N	0.98 ± 0.08	(1.7 ± 0.1) × 10^{-2}	18 ± 1
S289A	2.7 ± 0.2	9.0 ± 0.2	(3.4 ± 0.2) × 10^3

[a] The catalytic constants were determined with β-Asp-Leu as the substrate. The mutants were reconstituted with zinc.

Metal Analysis. The roles of the metal ions in the active site of IAD were probed by the preparation and reconstitution of apo-IAD with Zn^{2+}, Co^{2+}, Cd^{2+}, Ni^{2+}, and Mn^{2+}. The specific activity of apo-IAD was found to be less than 1% of that of the native enzyme when the metal content was reduced to an average of ∼0.07 equiv of Zn per active site. The reconstitution of apo-IAD with different divalent metal ions resulted in a differential recovery of catalytic activity depending on the specific metal ion utilized for this investigation. The highest specific activity was found with Zn, and lower levels of activity were found with Co, Cd, and Ni. No incorporation of Mn was found under the reaction conditions employed for this investigation. The reconstitution of the apo-IAD with zinc as the divalent cation was complete within 2 h, but the regain of catalytic activity was significantly slower with the other divalent cations. The approximate time for recovery of the maximum enzymatic activity was 15, 50, and 75 h for the Cd-, Ni-, and Co-substituted IAD, respectively. The average metal content per subunit of the reconstituted proteins was 2.0, 2.7, 2.9, and 1.4 for the Zn-, Co-, Cd-, and Ni-substituted forms of IAD, respectively. The kinetic constants obtained with substrate β-Asp-Leu are presented in Table 4.

pH−*Rate Profiles.* The effect of pH on the kinetic constants, k_{cat} and k_{cat}/K_m, was determined for the Zn-, Co-, Cd-, and Ni-substituted forms of IAD using β-Asp-Leu as the substrate. The pH−rate profiles for both kinetic constants are bell-shaped and indicate that one group must be unprotonated while another group must be protonated for optimum catalytic activity. The pH−rate profiles for the various metal-substituted forms of IAD are presented in Figures 3 and 4, and the kinetic constants from fits of the data to eq 2 are provided in Table 5. For k_{cat}/K_m, the kinetic pK_a for the group that must be unprotonated for activity is very much dependent on the specific metal ion that is bound to the active site. The lowest value of 5.3 was obtained with Co/Co-bound IAD, while the highest value of 7.7 was obtained with Cd/Cd-bound IAD. In contrast, the pK_a values for the group that must be protonated for catalytic activity did not vary as much with the substitution of divalent cations within the IAD active site.

Active Site-Directed Mutants of IAD. The roles of Glu77, Tyr137, Arg169, Arg233, Asp285, and Ser289 in the catalytic

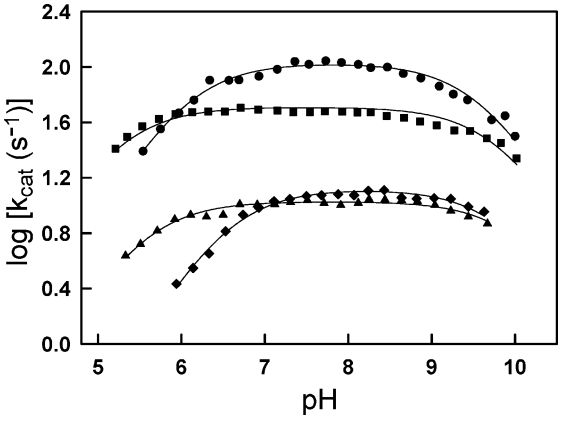

FIGURE 3: pH−rate profiles of k_{cat} for the metal-reconstituted forms of IAD. The kinetic constants were obtained for Zn (●), Co (■), Ni (▲), and Cd (◆). The data were fit to eq 2 using β-Asp-Leu as the substrate. Additional details are provided in the text and in Table 5.

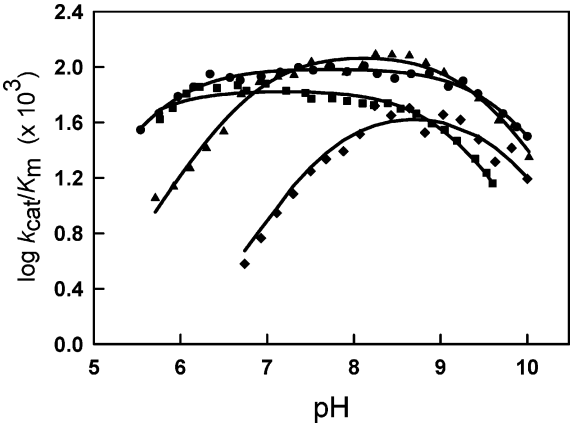

FIGURE 4: pH−rate profile of k_{cat}/K_m for the metal-reconstituted forms of IAD. The kinetic constants were obtained for Zn (●), Co (■), Ni (▲), and Cd (◆). The assays were conducted with β-Asp-Leu as the substrate, and the data were fit to eq 2. Additional details are provided in the text and in Table 5.

Table 5: pK_a Values for Metal-Substituted IAD from pH−Rate Profiles[a]

IAD	log k_{cat} vs pH		log k_{cat}/K_m vs pH	
	pK_1	pK_2	pK_1	pK_2
WT (Zn/Zn)	6.1 ± 0.1	9.6 ± 0.1	5.8 ± 0.1	9.7 ± 0.1
WT (Co/Co)	5.1 ± 0.2	9.8 ± 0.1	5.5 ± 0.1	9.2 ± 0.1
WT (Cd/Cd)	6.1 ± 0.1	10.5 ± 0.4	7.7 ± 0.1	9.7 ± 0.7
WT (Ni/Ni)	5.5 ± 0.1	10.5 ± 0.1	6.7 ± 0.1	9.4 ± 0.1

[a] The kinetic constants were determined with β-Asp-Leu as the substrate.

activity of IAD were probed by mutation of these residues to amino acids with alternative side chains. The mutant proteins were purified to homogeneity, and the zinc content varied from 1.3 to 2.0 per subunit. The kinetic constants for these mutant proteins were determined with the zinc-substituted form, and the results are presented in Table 4. The mutation of Glu77, Arg169, and Asp285 resulted in the largest diminutions in the catalytic constants relative to those of the wild-type enzyme.

Structure of the D285N Mutant Protein Complexed with β-Asp-His. The structure of the D285N mutant protein complexed with β-Asp-His was determined to 2.0 Å resolution and refined to an *R*-factor of 18.5%. Replacement of Asp285 with an asparagine resulted in less than full occupancies for the zinc ions. For the refinement of the model, the occupancies were set to 0.25 for both subunits in the asymmetric unit. In the first subunit of the asymmetric unit, is appears from the electron density that Lys162 is no longer carboxylated. The electron density for Lys162 in the second subunit, however, is consistent with a carboxyl group attached to the ϵ-nitrogen of its side chain. The substrate, β-Asp-His, is bound to both subunits in the asymmetric unit. Electron density corresponding to the bound substrate from subunit two is shown in Figure 5. Possible hydrogen bonding interactions between the protein and the ligand from subunit 2 are presented in Figure 6. The side chain of Glu77 interacts with the α-amino group of the β-Asp-His substrate, while the backbone amide groups of Gly75, Thr106, and Ser289 provide hydrogen bonding interactions with the α-carboxylate group of the ligand. The carbonyl moiety of β-Asp-His is positioned 2.4 Å from O^{η} of Tyr 137 and 2.4 Å from the β-metal. The guanidinium groups of Arg169 and Arg233 serve to anchor the carboxylate group of the histidine moiety to the protein. There are no interactions within 3.5 Å between the protein and the imidazole group of the β-Asp-His ligand. Other than reducing the metal content of the enzyme, the change from an aspartate at position 285 to an asparagine residue resulted in little overall structural perturbation. Nevertheless, the reduction in metal content and the decarboxylation of the modified K162 from one subunit in the asymmetric unit in the D285N mutant are probably caused by minor structural perturbations due to the loss of a direct metal ligand to M_{α}. The D285N protein−β-Asp-His and wild-type enzyme−aspartate complex models superimpose with a root-mean-square deviation of 0.16 Å for 382 structurally equivalent α-carbons.

DISCUSSION

Isoaspartyl dipeptidase catalyzes the hydrolysis of dipeptides formed from the β-carboxylate group of aspartic acid (*1*). The enzyme is specific for aspartate at the N-terminus of the dipeptide substrate but is relatively nonspecific for the amino acid occupying the C-terminal position. An analysis of the amino acid sequence and the three-dimensional structure of this enzyme has demonstrated that IAD is a member of the amidohydrolase superfamily. This diverse group of metalloproteins has been shown to catalyze the hydrolysis of amides and esters at carbon and phosphorus centers (*7*, *17*). The active sites of proteins within this enzyme superfamily contain a metal center that is either binuclear or mononuclear (*17*). The metal center found in the active site of IAD is binuclear and is similar to that previously described for phosphotriesterase (*18*), dihydroorotase (*19*), and urease (*20*), among others. Mechanistic investigations of the reactions catalyzed by these enzymes have demonstrated that the binuclear metal center is responsible for the activation of the nucleophilic water molecule and enhancement of the electrophilic character of the bond to be cleaved.

Substrate Specificity. Six different β-aspartyl dipeptides were tested for substrate turnover with IAD from *E. coli*. All of these compounds were found to be substrates with k_{cat} values that ranged from 1 to 200 s^{-1}. The k_{cat}/K_m of ~10^5 M^{-1} s^{-1} determined for β-Asp-Leu was the greatest of the compounds that were tested, whereas the turnover number for β-Asp-Ala was the highest. Since the side chains for the

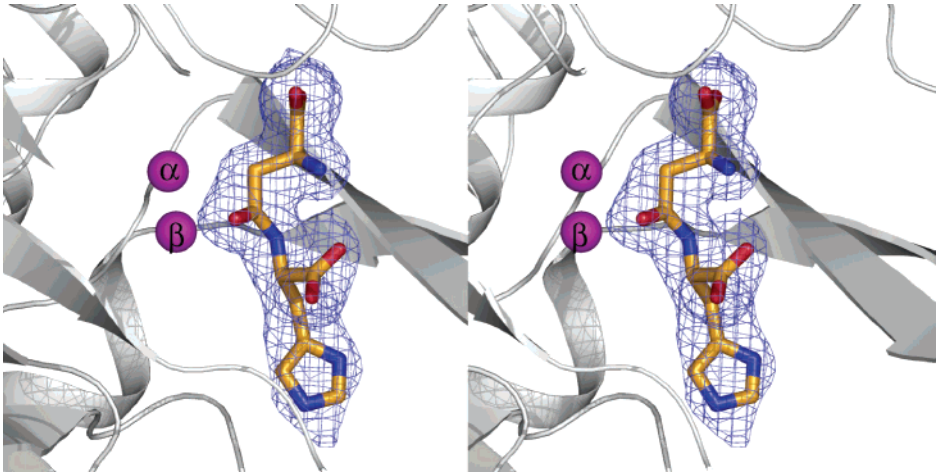

FIGURE 5: Structure of the D285N mutant protein of IAD complexed with β-Asp-His. Shown is the electron density corresponding to the bound ligand in subunit 2 of the asymmetric unit. The map was calculated with $F_o - F_c$ coefficients, where F_o was the native structure factor amplitude and F_c was the calculated structure factor amplitude from the model lacking the coordinates for the ligand. The map was contoured at 3σ.

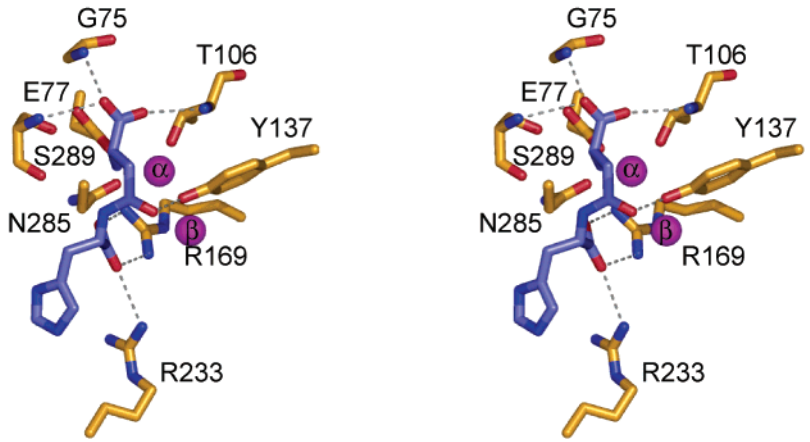

FIGURE 6: Potential hydrogen bonding interactions between β-Asp-His and the mutant D285N are represented by the dashed lines for subunit 2 of the asymmetric unit.

amino acids at the C-terminus of the dipeptides found to be substrates contain hydrophobic, aromatic, and hydrophilic substituents, the environment for the active site that accommodates this part of the substrate cannot be highly specific for a limited number of dipeptides. In the X-ray structure of β-Asp-His bound to the D285N mutant enzyme, the imidazole side chain of the substrate is not within 3.5 Å of any protein atoms. Only the side chains of Arg233 and Ile257 and the backbone carbonyl oxygen of Pro291 are within 4.0 Å of the imidazole side chain.

The purified IAD was able to hydrolyze α-Asp-Leu (**II**) with a k_{cat}/K_m of $\sim 10^3$ M^{-1} s^{-1}. This result demonstrates that the positioning of the α-amino group within the substrate can be shifted between C_2 and C_3 of the aspartate moiety with partial retention of catalytic activity. The X-ray structure of the bound β-Asp-His substrate within the active site of the sluggish D285N mutant protein demonstrates that the α-amino substituent of this substrate is ion-paired with the side chain carboxylate of Glu77 (Figure 6). In the structure of the wild-type IAD bound to the phosphonate analogue of α-Asp-Leu, the α-amino group of the inhibitor is positioned in a manner similar to that found with the β-Asp-His substrate bound to the D285N mutant enzyme (*21*). This observation demonstrates that the binding of the phosphonate analogue of α-Asp-Leu is accommodated within the active site of the wild-type enzyme by repositioning of the β-carboxylate of the inhibitor to a conformation that permits the ion pairing of the α-amino group with the side carboxylate of Glu77. This reorientation is possible since the free carboxylate group of the aspartate moiety of the β-Asp-His substrate is not strongly ion paired with any other residue within the active site of the protein, although there appear to be hydrogen bonding interactions between the backbone amide groups of Gly75, Thr106, and Ser289 and the α-carboxylate of β-Asp-His in the structure of the D285N mutant protein. Nevertheless, the α-amino group of the aspartate moiety is required for substrate activity since succinyl-Leu (**III**) is not a substrate and a relatively poor inhibitor of IAD. Moreover, the α-carboxylate of a β-aspartyl dipeptide is required for catalytic activity since β-Ala-Ala (**IV**) is not a substrate for the enzyme.

The α-carboxylate group from the amino acid at the C-terminus of a dipeptide substrate is ion paired with the two guanidinium groups from Arg169 and Arg233 as indicated in Figure 6. The importance of these interactions was tested by mutation of the two arginine residues to lysine and methionine. When either of these arginine residues is mutated to a lysine residue, the K_m value is substantially elevated and k_{cat} is reduced accordingly. However, the reduction in catalytic prowess is larger with changes to

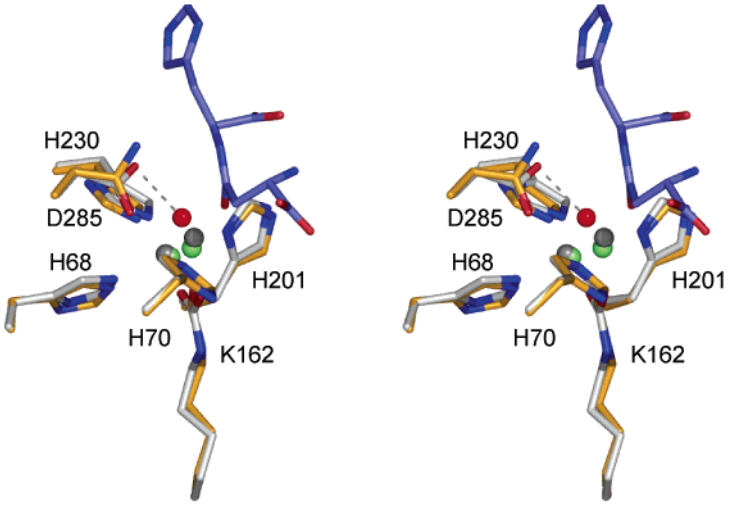

FIGURE 7: Superposition of the resting and substrate-bound forms of IAD. Side chains of the resting enzyme are depicted with white bonds, while those of the D285N−substrate complex mutant protein for subunit 2 of the asymmetric unit are displayed in gold. The positions of the zinc ions in the resting and D285N proteins are indicated by the gray and lime spheres, respectively, while the substrate is highlighted with blue bonds. The solvent molecule that bridges the binuclear metal center in the resting enzyme is drawn as a red sphere and sits on the *re* face of the ligand. The hydrogen bond between the carboxylate of Asp285 and the bridging solvent in the resting enzyme is represented by the dashed line.

Arg169 than to Arg233. In fact, when Arg169 is mutated to a methionine residue, the value of k_{cat}/K_m is reduced by more than 6 orders of magnitude relative to that of the wild-type enzyme. The R233M mutant retains significantly more activity.

Activation of Water. In the resting form of the wild-type enzyme, the only molecule from solvent that is bound to either metal ion in the active site is the one that serves as the bridge between the two metal ions (*3*). In the structure of the enzyme with bound aspartate, the β-carboxylate group is found ligated between the two metal ions as shown in Figure 2. One of the carboxylate oxygens is 2.3 Å from the β-metal, while the other oxygen is 2.8 Å from the α-metal ion. Taken together, these two structures demonstrate that the hydrolytic nucleophile most likely originates from the hydroxide and/or water that is originally bound between the two metal ions. These results also indicate that the β-carboxylate group of the aspartate product acts as a bridging ligand between the two divalent cations at the conclusion of the enzymatic reaction.

It is uncertain whether the solvent molecule that bridges the two divalent cations in the resting enzyme is water or hydroxide, and pH−rate profiles were used to address this question. With the wild-type enzyme, the pH−rate profiles for either k_{cat} or k_{cat}/K_m show that one group must be protonated for full catalytic activity while another group must be unprotonated. The loss of catalytic activity at low pH is consistent with the protonation of a bridging hydroxide to water. If this assumption is correct, then it is expected that the kinetic pK_a obtained from the pH−rate profiles will be a function of the specific metal ion bound to the active site. When the native metal ion zinc is replaced with cadmium, the kinetic pK_a for k_{cat}/K_m increases from 5.8 to 7.7. To a first approximation, this ionization represents the protonation of the bridging hydroxide in the absence of substrate and the subsequent loss of catalytic activity. This trend is consistent with the ionization of a metal-bound water molecule that gives rise to the active form of the enzyme. In aqueous systems, the pK_a of water bound to Zn^{2+} is 8.9, whereas it is 10.1 when water is bound to Cd^{2+} (*22*). In addition, a biomimetic chemical analogue of a binuclear Zn^{2+} complex has been reported to have a pK_a for the bridging hydroxide of 6.8 (*23*). The kinetic pK_a values measured for the catalytic activity of phosphotriesterase (*24*) and dihydroorotase (*25*) as a function of pH are also dependent on the specific divalent cation bound to the active site.

In contrast, the kinetic pK_a for the group that must be protonated for activity remains relatively insensitive to changes in the divalent cation for k_{cat}/K_m. The average value for this ionization is 9.5 ± 0.2, and thus, the loss of activity at high pH is highly likely to originate from the ionization of the α-amino group of the dipeptide substrate. The reported pK_a values for the ionization of the free α-amino groups of single amino acids vary from 9.2 to 9.7 (*26*). Further support for this conclusion is provided by the inability of succinylleucine (**III**) to serve as a substrate for IAD. Moreover, the α-amino group of the bound substrate in the D285N mutant protein is found to be ion-paired with the side chain carboxylate of Glu77. Confirmation of the importance of the ion pair between the side chain carboxylate of Glu77 and the α-amino group of the substrate derives from the catalytic properties of the E77D and E77Q mutants. In either case, the values of k_{cat} and k_{cat}/K_m are reduced by approximately 4 orders of magnitude when the side chain of Glu77 is modified. The α-amino group of the aspartate moiety in the wild-type−product complex (*3*) interacts with the backbone carbonyl and side chain hydroxyl of Ser289 as indicated in Figure 2. Site-directed mutagenesis of Ser289 to alanine diminishes the catalytic activity by ~2 orders of magnitude and suggests that the interaction of Ser 289 is important but not vital for catalysis and substrate binding.

Activation of the Substrate. The substrate can be activated for nucleophilic attack through a direct interaction with the binuclear metal center. Polarization of the carbonyl group of the bond to be cleaved via ligation to one or both of the metal ions would enhance the electrophilic character of the carbonyl carbon of the substrate. In the X-ray structure of the β-Asp-His substrate coordinated to the binuclear metal

center of the D285N mutant enzyme, the carbonyl oxygen of the scissile bond is coordinated to the β-metal ion at a distance of 2.4 Å. Similar enzyme−ligand interactions within the Michaelis complexes of bound substrates and inhibitors have previously been observed with other members of the amidohydrolase superfamily members, including phosphotriesterase (*27*), dihydroorotase (*19*), and urease (*20*, *28*). In all four enzymes, the conserved function for the β-metal ion within the binuclear metal center is polarization of the carbonyl or phosphoryl bond via Lewis acid catalysis.

Activation of the Leaving Group. During the course of hydrolysis of the peptide bond, the amide nitrogen of the incipient product must be protonated. With the homologous enzyme, dihydroorotase, the residue that appears to be responsible for protonation of the leaving group is the Asp250 that coordinates the α-metal ion within the binuclear center (*19*). In IAD, the homologous residue is Asp285. In the X-ray structure of IAD in the absence of bound ligands, the side chain carboxylate of Asp285 is in position to hydrogen bond to the hydroxide that bridges the two divalent cations as shown in Figure 7. The mutation of Asp285, to alanine or asparagine, results in a protein with very little enzymatic activity, and this result confirms the critical function of this residue. Indeed, it was possible to trap the substrate in the active site of the D285N mutant protein as shown in Figures 5 and 6. The orientation of the bound substrate in this inactive complex is in position to be attacked by the bridging hydroxide. Superposition of the mutant enzyme structure onto that of the resting wild-type enzyme is displayed in Figure 7. The bridging oxygen of the bound hydroxide in the resting enzyme is poised to utilize one set of lone pair electrons to attack the *re* face of the amide bond of the bound substrate. It is proposed that this reaction is facilitated by the abstraction of the proton from the hydroxide by the side chain carboxylate from Asp285. The protonated carboxylate is then in a position to donate the hydrogen to the leaving group amine upon subsequent cleavage of the C−N bond of the dipeptide substrate.

Mechanism of Action. The X-ray structures of IAD and the catalytic properties of the mutant and wild-type enzymes can be utilized to formulate a self-consistent reaction mechanism for the hydrolysis of β-aspartyl dipeptides. In the resting state of the enzyme, the two divalent cations are bound in a manner that accommodates the binding of hydroxide between the two metal ions. The hydroxide is hydrogen bonded to the side chain carboxylate of Asp285 that is also ligated to the α-metal ion within the active site of IAD. Substrates bind to the active site in a manner that positions the carbonyl oxygen adjacent to the β-metal ion. This interaction polarizes the carbonyl group and enhances the electrophilic character of the carbon to be attacked. The binding of β-aspartyl dipeptides to the active site is facilitated by an ion pair interaction between the side chain carboxylate of Glu77 and the α-amino substituent of the substrate and additional ion pair interactions between the α-carboxylate of the leaving group product and the guanidinium groups of Arg169 and Arg233. The enzymatic reaction is initiated by nucleophilic attack at the *re* face of the amide bond concomitant with proton transfer from the hydroxide to the side chain carboxylate of Asp285. A transient tetrahedral intermediate is formed that subsequently collapses with cleavage of the C−N bond via proton transfer from Asp285 to the α-amino group of the departing amino acid product. The reaction concludes with the newly formed carboxylate from the dipeptide coordinated to the binuclear metal center. The products depart the active site, and the binuclear metal center is recharged with hydroxide via a mechanism that has not been addressed in this investigation. The proposed reaction mechanism is outlined in Scheme 3. This transformation is analogous to the mechanisms that have previously been established for phosphotriesterase (*24*) and dihydroorotase (*19*, *25*).

Scheme 3

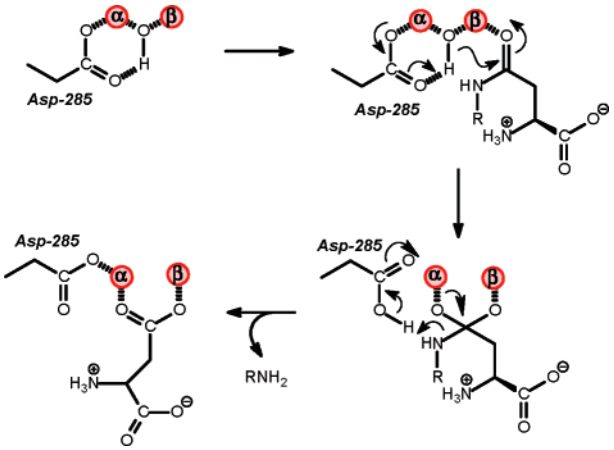

REFERENCES

1. Haley, E. E. (1968) Purification and properties of a β-aspartyl peptidase from *Escherichia coli*, *J. Biol. Chem. 243*, 5748−5752.
2. Gary, J. D., and Clarke, S. (1995) Purification and characterization of an isoaspartyl dipeptidase from *Escherichia coli*, *J. Biol. Chem. 270*, 4076−4087.
3. Thoden, J. B., Marti-Arbona, R., Raushel, F. M., and Holden, H. M. (2003) High-resolution X-ray structure of isoaspartyl dipeptidase from *Escherichia coli*, *Biochemistry 42*, 4874−4882.
4. Abendroth, J., Niefind, K., and Schomburg, D. (2002) X-ray structure of a dihydropyrimidinase from *Thermus* sp. at 1.3 Å resolution, *J. Mol. Biol. 320*, 143−156.
5. Cheon, Y. H., Kim, H. S., Han, K. H., Abendroth, J., Niefind, K., Schomburg, D., Wang, J., and Kim, Y. (2002) Crystal structure of D-hydantoinase from *Bacillus stearothermophilus*: Insight into the stereochemistry of enantioselectivity, *Biochemistry 41*, 9410−9417.
6. Xu, Z., Liu, Y., Yang, Y., Jiang, W., Arnold, E., and Ding, J. (2003) Crystal structure of D-hydantoinase from *Burkholderia pickettii* at a resolution of 2.7 angstroms: Insights into the molecular basis of enzyme thermostability, *J. Bacteriol. 185*, 4038−4049.
7. Gerlt, J. A., and Raushel, F. M. (2003) Evolution of function in $(\beta/\alpha)_8$-barrel enzymes, *Curr. Opin. Chem. Biol. 7*, 252−264.
8. Brynes, S., Burckart, G. J., and Mokotoff, M. (1978) Potential inhibitors of L-asparagine biosynthesis. 4. Substituted sulfonamide and sulfonylhydrazide analogues of L-asparagine, *J. Med. Chem. 21*, 45−49.
9. Hejazi, M., Piotukh, K., Mattow, J., Deutzmann, R., Volkmer-Engert, R., and Lockau, W. (2002) Isoaspartyl dipeptidase activity of plant-type asparaginases, *Biochem. J. 364*, 129−136.
10. Fresquet, V., Williams, L., and Raushel, F. M. (2004) Mechanism of cobyrinic acid *a,c*-diamide synthetase from *Salmonella typhimurium* LT2, *Biochemistry 43*, 10619−10627.
11. Schmidt, D. M., Hubbard, B. K., and Gerlt, J. A. (2001) Evolution of enzymatic activities in the enolase superfamily: Functional assignment of unknown proteins in *Bacillus subtilis* and *Escherichia coli* as L-Ala-D/L-Glu epimerases, *Biochemistry 40*, 15707−15715.
12. Cleland, W. W. (1979) Statistical analysis of enzyme kinetic data, *Methods Enzymol. 63*, 103−138.
13. Kabsch, W. (1988) Automatic indexing of rotation diffraction patterns, *J. Appl. Crystallogr. 21*, 67−71.

14. Kabsch, W. (1988) Evaluation of single-crystal X-ray diffraction data from a position sensitive detector, *J. Appl. Crystallogr. 21*, 916−924.
15. Tronrud, D. E., Ten Eyck, L. F., and Matthews, B. W. (1987) An efficient general-purpose least-squares refinement program for macromolecular structures, *Acta Crystallogr. A43*, 489−501.
16. Gary, J. D., and Clarke, S. (1998) β-Aspartyl dipeptidase, in *Handbook of Proteolytic Enzymes*, pp 1461−1465, Academic Press, London.
17. Holm, L., and Sander, C. (1997) An evolutionary treasure: Unification of a broad set of amidohydrolases related to urease, *Proteins 28*, 72−82.
18. Benning, M. M., Shim, H., Raushel, F. M., and Holden, H. M. (2001) High-resolution X-ray structures of different metal-substituted forms of phosphotriesterase from *Pseudomonas diminuta*, *Biochemistry 40*, 2712−2722.
19. Thoden, J. B., Phillips, G. N., Jr., Neal, T. M., Raushel, F. M., and Holden, H. M. (2001) Molecular structure of dihydroorotase: A paradigm for catalysis through the use of a binuclear metal center, *Biochemistry 40*, 6989−6997.
20. Jabri, E., Carr, M. B., Hausinger, R. P., and Karplus, P. A. (1995) The crystal structure of urease from *Klebsiella aerogenes*, *Science 268*, 998−1004.
21. Jozic, D., Kaiser, J. T., Huber, R., Bode, W., and Maskos, K. (2003) X-ray structure of isoaspartyl dipeptidase from *E. coli*: A dinuclear zinc peptidase evolved from amidohydrolases, *J. Mol. Biol. 332*, 243−256.
22. Barnum, D. W. (1983) Hydrolysis of cations. Formation constants and standard free energies of formation of hydroxy complexes. *Inorg. Chem. 22*, 2297−2305.
23. He, C., and Lippard, S. J. (2000) Modeling carboxylate-bridged dinuclear active site in metalloenzymes using a novel naphthyridine-based dinucleating ligand, *J. Am. Chem. Soc. 122*, 184−185.
24. Aubert, S. D., Li, Y., and Raushel, F. M. (2004) Mechanism for the hydrolysis of organophosphates by the bacterial phosphotriesterase, *Biochemistry 43*, 5707−5715.
25. Porter, T. N., Li, Y., and Raushel, F. M. (2004) Mechanism of the dihydroorotase reaction, *Biochemistry 43*, 16285−16292.
26. Dawson, R. M. C., Elliott, D. C., Elliott, W. H., and Jones, K. M. (1986) *Data for Biochemical Research*, 3rd ed., pp 1−31, Oxford Science Publications, Oxford, U.K.
27. Benning, M. M., Hong, S. B., Raushel, F. M., and Holden, H. M. (2000) The binding of substrate analogs to phosphotriesterase, *J. Biol. Chem. 275*, 30556−30560.
28. Benini, S., Rypniewski, W. R., Wilson, K. S., Miletti, S., Ciurli, S., and Mangani, S. (1999) A new proposal for urease mechanism based on the crystal structures of the native and inhibited enzyme from *Bacillus pasteurii*: Why urea hydrolysis costs two nickels, *Struct. Folding Des. 7*, 205−216.

BI050008R